Recognizing Landmarks in Large-Scale Social Image Collections

David J. Crandall, Yunpeng Li, Stefan Lee, and Daniel P. Huttenlocher

Abstract The dramatic growth of social media websites over the last few years has created huge collections of online images and raised new challenges in organizing them effectively. One particularly intuitive way of browsing and searching images is by the geo-spatial location of where on Earth they were taken, but most online images do not have GPS metadata associated with them. We consider the problem of recognizing popular landmarks in large-scale datasets of unconstrained consumer images by formulating a classification problem involving nearly 2 million images and 500 categories. The dataset and categories are formed automatically from geotagged photos from Flickr by looking for peaks in the spatial geotag distribution corresponding to frequently photographed landmarks. We learn models for these landmarks with a multiclass support vector machine, using classic vector-quantized interest point descriptors as features. We also incorporate the non-visual metadata available on modern photo-sharing sites, showing that textual tags and temporal constraints lead to significant improvements in classification rate. Finally, we apply recent breakthroughs in deep learning with Convolutional Neural Networks, finding that these models can dramatically outperform the traditional recognition approaches to this problem, and even beat human observers in some cases.[1]

David J. Crandall
Indiana University, Bloomington, Indiana USA, e-mail: djcran@indiana.edu

Yunpeng Li
École Polytechnique Fédérale de Lausanne, 1015 Lausanne, Switzerland, e-mail: yunpeng.li@epfl.ch

Stefan Lee
Indiana University, Bloomington, Indiana USA, e-mail: steflee@indiana.edu

Daniel P. Huttenlocher
Cornell University, Ithaca, New York USA, e-mail: dph@cs.indiana.edu

[1] This is an expanded and updated version of an earlier conference paper [23].

1 Introduction

Online photo collections have grown dramatically over the last few years, with Facebook alone now hosting over 250 billion images [2]. Unfortunately, techniques for automatic photo organization and search have not kept pace, with most modern photo-sharing sites using simple techniques like keyword search based on text tags provided by users. In order to allow users to browse and search huge image collections more efficiently we need algorithms that can automatically recognize image content and organize large-scale photo collections accordingly.

A natural way of organizing photo collections is based on geospatial location — where on Earth an image was taken. This allows people to search for photos taken near a particular spot of interest, or to group images based on similar locations or travel itineraries. To enable this type of organization, geospatial coordinates or 'geo-tags' can be encoded in the metadata of a photo, and Global Positioning System (GPS) receivers embedded in modern smartphones and high-end cameras can record these positions automatically when a photo is captured. However, the vast majority of online photos are not geo-tagged, and even when available, geo-tags are often incorrect due to GPS error or other noise [15].

Recognizing where a photo was taken based on its visual content is thus an important problem. Besides the potential impact on geo-localization, this is an interesting recognition problem in and of itself. Unlike many tasks like scene type recognition or tag suggestion, which are inherently subjective, place recognition is a uniquely well-posed problem; except for pathological cases like synthetic images or photos taken from space, every photo is taken at exactly one point on Earth, and so there is exactly one correct answer. Moreover, it is relatively easy to assemble large-scale training and test data for this problem by using geo-tagged images from social media sites like Flickr. This is in contrast to most other recognition problems in which producing ground truth data involves extensive manual labor, which historically has limited the size of datasets and introduced substantial bias [38].

In this chapter we consider the problem of classifying consumer photos according to where on Earth they were taken, using millions of geo-tagged online images to produce labeled training data with no human intervention. We produce this dataset by starting with a collection of over 30 million public geo-tagged images from Flickr. We use this dataset both to define a set of category labels, as well as to assign a ground truth category to each training and test image. The key observation underlying our approach is that when many different people take photos at the same place, they are likely photographing some common area of interest. We use a mean shift clustering procedure [4] to find hotspots or peaks in the spatial distribution of geotagged photos, and then use large peaks to define the category labels. We then assign any photos geo-tagged within a peak to the same category label.

We call each localized hotspot of photographic activity a *landmark*. Most of our landmarks do not consist of a single prominent object; for example, many are museums, with photos of hundreds of different exhibits as well as photos containing little or no visual evidence of the landmark itself (e.g. close-ups of people's faces). We could use visual or textual features of images to try to divide these complex landmarks into individual objects, as others have done [42], but we purposely choose not to do this; by defining the labels using only geo-tags, we ensure that the features used for testing classification algorithms (namely visual content, text tags, and timestamps) do not also bias the category labels. However, because we do not try to remove outliers or difficult images, the photographs taken at these landmarks are quite diverse (see Figure 1 for some examples), meaning the labeled test datasets are noisy and challenging. Our landmark classification task is thus more similar to object category recognition than to specific object recognition. In Section 3 we discuss the details of our dataset collection approach.

Once we have assembled a large dataset of millions of images and hundreds of categories, we present and evaluate techniques for classifying the landmark at which each photo was taken. We first apply multiclass Support Vector Machines (SVMs) [5] with features based on classic bags of vector-quantized invariant feature point descriptors [8, 25]. Social photo collections also contain sources of non-visual evidence that can be helpful for classification; for instance, social ties have been found to improve face recognition [36] and image tagging [27]. We explore incorporating the free-form text tags that Flickr users add to some photos. We also incorporate temporal evidence, using the fact that most people take series of photos over time (for instance, as they move about the tourist sites of a city). We thus analyze the *photo stream* of a given photographer, using Structured Support Vector Machines [40] to predict a sequence of category labels jointly rather than classifying a single photo at a time. Finally, inspired by the very recent success of deep learning techniques on a variety of recognition problems [20, 29, 37, 39], we apply Convolutional Neural Networks to our problem of landmark classification as an alternative to the more traditional bag-of-words models with hand-designed image features. Feature extraction, learning, and classification methods are discussed in Section 4.

In Section 5 we present a set of large-scale classification experiments involving between 10 and 500 categories and tens to hundreds of thousands of photos. We begin with the bag-of-words models of SIFT feature points, finding that the combination of image and text features performs better than either alone, and that visual features boost performance even for images that already have text tags. We also describe a small study of human accuracy on our dataset, to give a sense of the noise and difficulty of our task. We then show that using temporal context from photos taken by the same photographer nearby in time yields a significant improvement compared to using visual features alone — around 10 percentage points in most cases. Finally, we show that the neural nets give a further dramatic increase in performance, in some cases even beating humans, giving further evidence of the power of deep learning over traditional features on problems with large-scale datasets.

2 Related Work

Visual geolocation has received increasing attention in the last few years [14, 16, 19, 22–24, 30, 31, 35, 42] driven in part by the availability of cheap training and test data in the form of geo-tagged Flickr photos. We briefly highlight some of the work most related to this chapter here, but please see Luo *et al.* [26] for a more comprehensive survey. The IM2GPS paper of Hays and Efros [16] estimates a latitude-longitude coordinate estimate for an image by matching against a large dataset of geo-tagged photos from Flickr, identifying nearest neighbors and producing a geospatial probability distribution based on the matches. Our goal is different, as we do not try to predict location directly but rather just use location to derive category labels. (For instance, in our problem formulation a misclassification with a geographically proximate category is just as bad as with one that is far away.) Moreover, the IM2GPS test set contains only 237 images that were partially selected by hand, making it difficult to generalize the results beyond that set. In contrast we use automatically generated test sets that contain tens or hundreds of thousands of photos, providing highly reliable estimates of performance accuracy. Follow-up work by Kalogerakis *et al.* generalized IM2GPS to geo-localize a stream of multiple images at the same time by imposing constraints on human travel patterns [19].

Other papers have considered landmark classification tasks similar to the one we study here, although typically at a smaller scale. For example, Li *et al.* [22] study how to build a model of a landmark by extracting a small set of iconic views from a large set of photographs. The paper tests on three hand-chosen categories. Zheng *et al.* [42] have an approach similar to ours in that it finds highly photographed landmarks automatically from a large collection of geotagged photos. However, the test set they use is hand-selected and small — 728 total images for a 124-category problem, or fewer than 6 test images per category — and their approach is based on nearest-neighbor search, which may not scale to the millions of test images we consider here. Philbin *et al.* [30] study building recognition in the context of how to scale bag-of-features models using random vocabulary trees and fast geometric verification, testing on a dataset of 5,000 labeled images. Crandall *et al.* [6] study geographic embedding and organization of photos by clustering into landmarks and also study recognition, but at a much more limited scale (classifying among landmarks of a known city).

While we approach geo-localization as a recognition problem, an alternative is to study it in the context of 3D reconstruction [35]. If a 3D model of a place is available, then new images can be geo-localized very accurately, sometimes much more accurately than GPS [7]. But 3D reconstruction is computationally expensive, and is possible only in areas having dense coverage (typically thousands of images).

We apply several widely used recognition techniques to our landmark recognition problem, based on bag-of-words models of vector-quantized, invariant feature points [8, 25]. A very large body of literature has studied these models, including how to optimize them for accuracy and speed in different contexts and tasks: see Grauman and Leibe [12] for a comprehensive overview. We also apply Convolutional Neural Networks, which, in contrast, are arguably less well understood. Following the surprising success of deep Convolutional Neural Networks on the 2012 ImageNet recognition challenge [20], CNNs have been applied to a variety of computer vision tasks and have shown striking improvements over the state of the art [11, 21, 29, 32, 34, 37, 39, 41]. The main advantage of deep learning methods over more traditional techniques is that the image features can be learned along with the object models in a unified optimization problem, instead of using generic hand-designed features (like SIFT [25]), which are likely not optimal for most tasks. Of course, learning these features requires more data and more computational power; the resurgence of neural networks in computer vision is thanks in no small part to powerful GPUs and large annotated datasets (like the ones we have here).

3 Building an Internet-Scale Landmark Dataset

Social photo-sharing websites with their huge collections of publicly available, user-generated images and metadata have been a breakthrough in computer vision, giving researchers an economical way of collecting large-scale, realistic consumer imagery. However, when constructing datasets from Internet photo sources, it is critical to avoid potential biases either in selecting the images to include in the dataset, the categories to include in the classification task, or in assigning ground-truth labels to images. Biases of different types affect even the most popular vision datasets [38]. For instance, methods based on searching for photos tagged with hand-selected keywords (e.g., [16, 30]) are prone to bias, because one might inadvertently choose keywords corresponding to objects that are amenable to a particular image classification algorithm. Many researchers have also used unspecified or subjective criteria to choose which images to include in the dataset, again introducing the potential for bias towards a particular algorithm. Other object recognition datasets like PASCAL [10] and Caltech [13] have object classes that were selected by computer vision researchers, making it unclear whether these are the most important categories that should be studied. Also problematic is using the same kinds of features to produce ground-truth labels as are used by the classification algorithm [3,33,42]. Recent datasets like ImageNet [9] avoid many sources of bias by defining ground truth labels based on more principled approaches like semantic categories of WordNet [28], and by avoiding subconscious biases of computer vision researchers by crowd-sourcing labels with Mechanical Turk, but these approaches still require a huge amount of human labor.

We thus advocate automatic techniques for creating datasets based on properties of human activity, such as where pictures are taken, without manual intervention. To be most useful for training and testing of classifiers, the ground truth labels should be selected and produced in a way that is automatic and objective, based on sources other than the features used by the classifiers. Our approach is based on the observation that when many people take photos at the same location it is highly likely that these are photos of the same thing. We therefore define category labels by finding geospatial clusters of high photographic activity and assign all photos within that cluster the same label.

In particular, our dataset was formed by using Flickr's public API to retrieve metadata for over 60 million publicly accessible geotagged photos. We eliminated photos for which the precision of the geotags was worse than about a city block

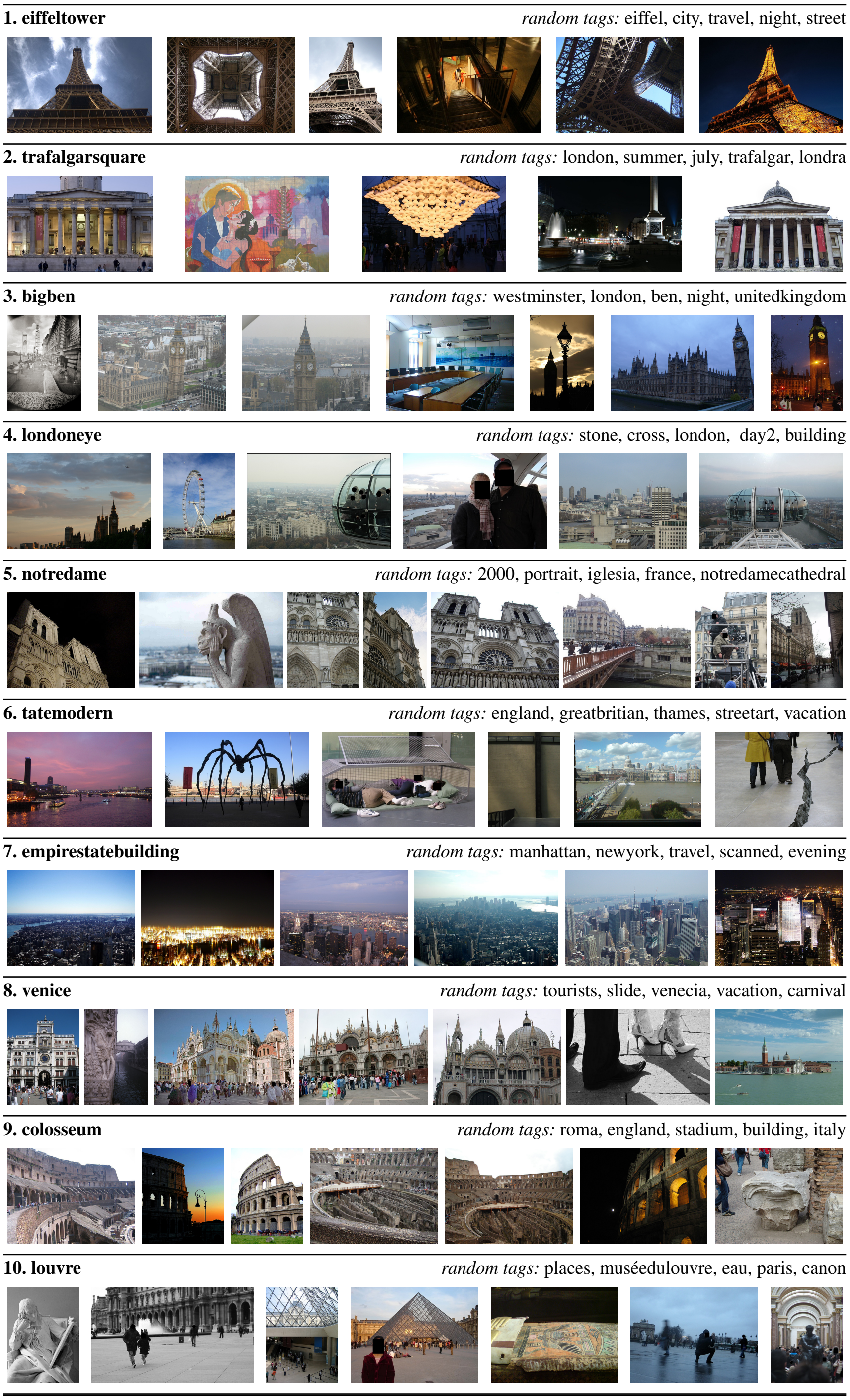

Fig. 1 The categories in our 10-way classification dataset, consisting of the 10 most photographed landmarks on Flickr. To illustrate the diversity and noise in our automatically generated dataset, we show five random images and five random text tags from each category. (We have obscured faces to protect privacy. The landmark tagged "venice" is Piazza San Marco.)

	Users	Geo-coordinate	Descriptive tags
1	4854	48.8584, 2.2943	eiffeltower, paris
2	4146	51.5080, -0.1281	trafalgarsquare, london
3	3442	51.5008, -0.1243	bigben, london
4	3424	51.5034, -0.1194	londoneye, london
5	3397	48.8531, 2.3493	cathedral, paris
6	3369	51.5080, -0.0991	tatemodern, london
7	3179	40.7485, -73.9854	empirestatebuilding, newyorkcity
8	3167	45.4340, 12.3390	venice, venezia
9	3134	41.8904, 12.4920	colosseum, rome
10	3081	48.8611, 2.3360	pyramid, paris
11	2826	40.7578, -73.9857	timessquare, newyorkcity
12	2778	40.7590, -73.9790	rockefeller, newyorkcity
13	2710	41.8828, -87.6233	cloudgate, chicago
14	2506	41.9024, 12.4574	vaticano, rome
15	2470	48.8863, 2.3430	sacrecoeur, paris
16	2439	51.5101, -0.1346	piccadillycircus, london
17	2321	51.5017, -0.1411	buckingham, london
18	2298	40.7562, -73.9871	timessquare, newyorkcity
19	2296	48.8738, 2.2950	arcdetriomphe, paris
20	2127	40.7526, -73.9774	grandcentralstation, newyorkcity
21	2092	41.8989, 12.4768	pantheon, rome
22	2081	41.4036, 2.1742	sagradafamilia, barcelona
23	2020	51.5056, -0.0754	towerbridge, london
24	1990	38.8894, -77.0499	lincolnmemorial, washingtondc
25	1983	51.5193, -0.1270	britishmuseum, london
26	1960	52.5164, 13.3779	brandenburggate, berlin
27	1865	51.5078, -0.0762	toweroflondon, london
28	1864	45.4381, 12.3357	rialto, venezia
29	1857	40.7641, -73.9732	applestore, newyorkcity
30	1828	47.6206, -122.3490	needle, seattle
31	1828	47.6089, -122.3410	market, seattle
32	1798	51.5013, -0.1198	bigben, london
33	1789	38.8895, -77.0406	wwii, washingtondc
34	1771	50.0873, 14.4208	praga, praha
35	1767	51.5007, -0.1263	bigben, london
36	1760	48.8605, 2.3521	centrepompidou, paris
37	1743	41.9010, 12.4833	fontanaditrevi, rome
38	1707	37.7879, -122.4080	unionsquare, sanfrancisco
39	1688	43.7731, 11.2558	duomo, firenze
40	1688	43.7682, 11.2532	pontevecchio, firenze
41	1639	36.1124, -115.1730	paris, lasvegas
42	1629	43.7694, 11.2557	firenze, firenze
43	1611	38.8895, -77.0353	washingtonmonument, washingtondc
44	1567	41.9023, 12.4536	basilica, rome
45	1505	51.5137, -0.0984	stpaulscathedral, london
46	1462	40.7683, -73.9820	columbuscircle, newyorkcity
47	1450	41.4139, 2.1526	parcguell, barcelona
48	1433	52.5186, 13.3758	reichstag, berlin
49	1419	37.8107, -122.4110	pier39, sanfrancisco
50	1400	51.5101, -0.0986	millenniumbridge, london
51	1391	41.8991, 12.4730	piazzanavona, rome
52	1379	41.9061, 12.4826	spanishsteps, rome
53	1377	37.8026, -122.4060	coittower, sanfrancisco
54	1369	40.6894, -74.0445	libertyisland, newyorkcity
55	1362	41.8953, 12.4828	vittoriano, rome
56	1359	51.5050, -0.0790	cityhall, london
57	1349	50.8467, 4.3524	grandplace, brussel
58	1327	48.8621, 2.2885	trocadero, paris
59	1320	36.1016, -115.1740	newyorknewyork, lasvegas
60	1318	48.8656, 2.3212	placedelaconcorde, paris
61	1320	41.9024, 12.4663	castelsantangelo, rome
62	1305	52.5094, 13.3762	potsdamerplatz, berlin
63	1297	41.8892, -87.6245	architecture, chicago
64	1296	40.7613, -73.9772	museumofmodernart, newyorkcity
65	1292	50.0865, 14.4115	charlesbridge, praha
66	1270	40.7416, -73.9894	flatironbuilding, newyorkcity
67	1260	48.1372, 11.5755	marienplatz, mnchen
68	1242	40.7792, -73.9630	metropolitanmuseumofart, newyorkcity
69	1239	48.8605, 2.3379	louvre, paris
70	1229	40.7354, -73.9909	unionsquare, newyorkcity
71	1217	40.7541, -73.9838	bryantpark, newyorkcity
72	1206	37.8266, -122.4230	prison, sanfrancisco
73	1196	40.7072, -74.0110	nyse, newyorkcity
74	1193	45.4643, 9.1912	cathedral, milano
75	1159	40.4155, -3.7074	plazamayor, madrid
76	1147	51.5059, -0.1178	southbank, london
77	1141	37.8022, -122.4190	lombardstreet, sanfrancisco
78	1127	37.7951, -122.3950	ferrybuilding, sanfrancisco
79	1126	-33.8570, 151.2150	sydneyoperahouse, sydney
80	1104	51.4996, -0.1283	westminsterabbey, london
81	1100	51.5121, -0.1229	coventgarden, london
82	1093	37.7846, -122.4080	sanfrancisco, sanfrancisco
83	1090	41.8988, -87.6235	hancock, chicago
84	1083	52.5141, 13.3783	holocaustmemorial, berlin
85	1081	50.0862, 14.4135	charlesbridge, praha
86	1077	50.0906, 14.4003	cathedral, praha
87	1054	41.3840, 2.1762	cathedral, barcelona
88	1042	28.4189, -81.5812	castle, waltdisneyworld
89	1034	38.8898, -77.0095	capitol, washingtondc
90	1024	41.3820, 2.1719	boqueria, barcelona
91	1023	48.8638, 2.3135	pontalexandreiii, paris
92	1022	41.8928, 12.4844	forum, rome
93	1021	40.7060, -73.9968	brooklynbridge, newyorkcity
94	1011	36.6182, -121.9020	montereybayaquarium, monterey
95	1009	37.9716, 23.7264	parthenon, acropolis
96	1008	41.3953, 2.1617	casamil, barcelona
97	986	43.6423, -79.3871	cntower, toronto
98	983	52.5099, 13.3733	sonycenter, berlin
99	972	34.1018, -118.3400	hollywood, losangeles
100	969	48.8601, 2.3263	museedorsay, paris

Table 1 The world's 100 most-photographed, landmark-sized hotspots as of 2009, according to our analysis of Flickr geo-tags, ranked by number of unique photographers. We use these hotspots to automatically define our landmark categories. For each landmark we show the number of photographers, the latitude-longitude coordinate of the hotspot centroid, and two automatically selected tags corresponding to the most distinctive tag (i.e. most-frequent relative to the worldwide background distribution) within the landmark region and within the surrounding city-scale region.

(precision score under 13 in the Flickr metadata). For each of the remaining 30 million photos, we considered its latitude-longitude coordinates as a point in the plane, and then performed a mean shift clustering procedure [4] on the resulting set of points to identify local peaks in the photo density distribution [6]. The radius of the disc used in mean shift allowed us to select the scale of the 'landmarks.' We used a radius of 0.001 degrees, which corresponds to roughly 100 meters at middle latitudes.[2] Since our goal is to identify locations where many *different* people took pictures, we count at most five photos from any given Flickr user towards any given peak, to prevent high-activity users from biasing the choice of categories. We currently use the top 500 such peaks as categories. After finding peaks, we rank them in decreasing order of the number of distinct photographers who have photographed the landmark. Table 1 shows the top 100 of these peaks, including the number of unique photographers, the geographic centroid of the cluster, and representative tags for each cluster. The tags were chosen automatically using the same technique as in [6], which looks for tags that occur very frequently on photos inside a geographic region but rarely outside of it.

We downloaded all 1.9 million photos known to our crawler that were geotagged within one of these 500 landmarks. For the experiments on classifying temporal photo streams, we also downloaded all images taken within 48 hours of any photo taken in a landmark, bringing the total dataset to about 6.5 million photos. The images were downloaded at Flickr's medium resolution level, about 0.25 megapixels. Figure 1 shows random images from each of the top 10 landmarks, showing the diversity of the dataset.

4 Landmark Recognition

We now consider the task of image classification in the large-scale image dataset produced using the procedure described above. Since our landmark categories were selected to be non-overlapping, these categories are mutually exclusive and thus each image has exactly one correct label. We first discuss how to classifying single images with bag-of-words models in Section 4.1, before turning to the temporal models in Section 4.2 and the deep learning-based methods in Section 4.3.

4.1 Single Image Classification Using Bag of Words Models

To perform image classification we adopt the bag-of-features model proposed by Csurka *et al.* [8], where each photo is represented by a feature vector recording occurrences of vector-quantized SIFT interest point descriptors [25]. As in that paper, we built a visual vocabulary by clustering SIFT descriptors from photos in the training set using the *k*-means algorithm. To prevent some images or categories from biasing the vocabulary, for the clustering process we sampled a fixed number of interest points from each image, for a total of about 500,000 descriptors. We used an efficient implementation of *k*-means using the approximate nearest neighbor (ANN) technique of [1] (to assign points to cluster centers during the expectation (E-step)

---

[2] Since longitude lines grow closer towards the poles, the spatial extent of our landmarks are larger at the equator than near the poles. We have not observed this to be a major problem because most population centers are near the middle latitudes, but future work could use better distance functions.

of k-means). The advantage of this technique over many others is that it guarantees an upper bound on the approximation error; we set the bound such that the cluster center found by ANN is within 110% of the distance from the point to the optimal cluster center.

Once a visual vocabulary of size k had been generated, a k-dimensional feature vector was constructed for each image by using SIFT to find local interest points and assigning each interest point to the visual word with the closest descriptor. We then formed a frequency vector which counted the number of occurrences of each visual word in the image. For textual features we used a similar vector space model in which any tag used by at least three different users was a dimension in the feature space, so that the feature vector for a photo was a binary vector indicating presence or absence of each text tag. Both types of feature vectors were L2-normalized. We also studied combinations of image and textual features, in which case the image and text feature vectors were simply concatenated after normalization.

We learned a linear model that scores a given photo for each category and assigns it to the class with the highest score. More formally, let m be the number of classes and $\mathbf{x}$ be the feature vector of a photo. Then the predicted label is

$$\hat{y} = arg\,max_{y\in\{1,\cdots,m\}} s(\mathbf{x}, y; \mathbf{w}), \tag{1}$$

where $\mathbf{w} = (\mathbf{w}_1^T, \cdots, \mathbf{w}_m^T)^T$ is the model and $s(\mathbf{x}, y; \mathbf{w}) = \langle \mathbf{w}_y, \mathbf{x} \rangle$ is the score for class y under the model. Note that in our settings, the photo is always assumed to belong to one of the m categories. Since this is by nature a multi-way (as opposed to binary) classification problem, we use multiclass SVMs [5] to learn the model $\mathbf{w}$, using the SVM^{multiclass} software package [18]. For a set of training examples $\{(\mathbf{x}_1, y_1), \cdots, (\mathbf{x}_N, y_N)\}$, our multiclass SVM optimizes an objective function,

$$\begin{aligned} &\min_{\mathbf{w},\boldsymbol{\xi}} \frac{1}{2} \|\mathbf{w}\|^2 + C \sum_{i=1}^{N} \xi_i \\ &\text{s.t. } \forall i, y \neq y_i : \langle \mathbf{w}_{y_i}, \mathbf{x}_i \rangle - \langle \mathbf{w}_y, \mathbf{x}_i \rangle \geq 1 - \xi_i, \end{aligned} \tag{2}$$

where C is the trade-off between training performance and margin in SVM formulations (which we simply set to $\bar{x}^{-2}$ where $\bar{x}$ is the average L2-norm of the training feature vectors). Hence for each training example, the learned model is encouraged to give higher scores to the correct class label than to the incorrect ones. By rearranging terms it can be shown that the objective function is an upper bound on the training error.

In contrast, many previous approaches to object recognition using bag-of-parts models (such as Csurka *et al.* [8]) trained a set of binary SVMs (one for each category) and classified an image by comparing scores from the individual SVMs. Such approaches are problematic for n-way, forced-choice problems, however, because the scores produced by a collection of independently trained binary SVMs may not be comparable, and thus lack any performance guarantee. It is possible to alleviate this problem by using a different C value for each binary SVM [8], but this introduces additional parameters that need to be tuned, either manually or via cross validation. Here we use multiclass SVMs, because they are inherently suited for multi-category classification.

Note that while the categories in this single-photo classification problem correspond to geographic locations, there is no geographical information used during the actual learning or classification. For example, unlike IM2GPS [16], we are not concerned with pinpointing a photo on a map, but rather with classifying images into discrete categories which happen to correspond to geospatial positions.

4.2 Incorporating Temporal Information

Photos taken by the same photographer at nearly the same time are likely to be related. In the case of landmark classification, constraints on human travel mean that certain sequences of category labels are much more likely than others. To learn the patterns created by such constraints, we view temporal sequences of photos taken by the same user as a single entity and consider them jointly as a structured output.

4.2.1 Temporal Model for Joint Classification

We model a temporal sequence of photos as a graphical model with a chain topology, where the nodes represent photos, and edges connect nodes that are consecutive in time. The set of possible labels for each node is simply the set of m landmarks, indexed from 1 to m. The task is to label the entire sequence of photos with category labels, however we score correctness only for a single selected photo in the middle of the sequence, with the remaining photos serving as temporal context for that photo. Denote an input sequence of length n as $X = ((\mathbf{x}_1, t_1), \cdots, (\mathbf{x}_n, t_n))$, where $\mathbf{x}_v$ is a feature vector for node v (encoding evidence about the photo such as textual tags or visual information) and t_v is the corresponding timestamp. Let $Y = (y_1, \cdots, y_n)$ be a labeling of the sequence. We would like to express the scoring function $S(X, Y; \mathbf{w})$ as the inner product of some *feature map* $\Psi(X, Y)$ and the model parameters $\mathbf{w}$, so that the model can be learned efficiently using the structured SVM.

Node Features. To this end, we define the feature map for a single node v under the labeling as,

$$\Psi_V(\mathbf{x}_v, y_v) = (I(y_v = 1)\mathbf{x}_v^T, \cdots, I(y_v = m)\mathbf{x}_v^T)^T, \tag{3}$$

where $I(\cdot)$ is an indicator function. Let $\mathbf{w}_V = (\mathbf{w}_1^T, \cdots, \mathbf{w}_m^T)$ be the corresponding model parameters with $\mathbf{w}_y$ being the weight vector for class y. Then the node score $s_V(\mathbf{x}_v, y_v; \mathbf{w}_V)$ is the inner product of the $\Psi_V(\mathbf{x}_v, y_v)$ and $\mathbf{w}_V$,

$$s_V(\mathbf{x}_v, y_v; \mathbf{w}_V) = \langle \mathbf{w}_V, \Psi_V(\mathbf{x}_v, y_v) \rangle . \tag{4}$$

Edge Features. The feature map for an edge (u,v) under labeling Y is defined in terms of the labels y_u and y_v, the time elapsed between the two photos $\delta t = |t_u - t_v|$, and the speed required to travel from landmark y_u to landmark y_v within that time, $speed(\delta t, y_u, y_v) = distance(y_u, y_v)/\delta t$. Since the strength of the relation between two photos decreases with the elapsed time between them, we divide the full range of δt into M intervals $\Omega_1, \cdots, \Omega_M$. For δt in interval Ω_τ, we define a feature vector,

$$\psi_\tau(\delta t, y_u, y_v) = (I(y_u = y_v), I(speed(\delta t, y_u, y_v) > \lambda_\tau))^T, \tag{5}$$

where λ_τ is a speed threshold. This feature vector encodes whether the two consecutive photos are assigned the same label and, if not, whether the transition requires a person to travel at an unreasonably high speed (i.e. greater than λ_τ). The exact choice of time intervals and speed thresholds are not crucial. We also take into consideration the fact that some photos have invalid timestamps (e.g. a date in the 22nd century) and define the feature vector for edges involving such photos as,

$$\psi_0(t_u, t_v, y_u, y_v) = I(y_u = y_v)(I(z = 1), I(z = 2))^T, \tag{6}$$

where z is 1 if exactly one of t_u or t_v is invalid and 2 if both are. Here we no longer consider the speed, since it is not meaningful when timestamps are invalid. The complete feature map for an edge is thus,

$$\begin{aligned}\Psi_E(t_u, t_v, y_u, y_v) = (&I(\delta t \in \Omega_1)\psi_1(\delta t, y_u, y_v)^T, \cdots, I(\delta t \in \Omega_M)\psi_M(\delta t, y_u, y_v)^T, \\ &\psi_0(t_u, t_v, y_u, y_v)^T)^T\end{aligned} \tag{7}$$

and the edge score is,

$$s_E(t_u, t_v, y_u, y_v; \mathbf{w}_E) = \langle \mathbf{w}_E, \Psi_E(t_u, t_v, y_u, y_v) \rangle, \tag{8}$$

where $\mathbf{w}_E$ is the vector of edge parameters.

Overall Feature Map. The total score of input sequence X under labeling Y and model $\mathbf{w} = (\mathbf{w}_V^T, \mathbf{w}_E^T)^T$ is simply the sum of individual scores over all the nodes and edges. Therefore, by defining the overall feature map as,

$$\Psi(X,Y) = (\sum_{v=1}^{n} \Psi_V(\mathbf{x}_v, y_v)^T, \sum_{v=1}^{n-1} \Psi_E(t_v, t_{v+1}, y_v, y_{v+1})^T)^T,$$

the total score becomes an inner product with $\mathbf{w}$,

$$S(X,Y;\mathbf{w}) = \langle \mathbf{w}, \Psi(X,Y) \rangle. \tag{9}$$

The predicted labeling for sequence X by model $\mathbf{w}$ is one that maximizes the score,

$$\hat{Y} = arg\,max_{Y \in \mathscr{Y}_X} S(X,Y;\mathbf{w}), \tag{10}$$

where $\mathscr{Y}_X = \{1, \cdots, m\}^n$ is the the label space for sequence X of length n. This can be obtained efficiently using Viterbi decoding, because the graph is acyclic.

4.2.2 Parameter Learning

Let $((X_1, Y_1), \cdots, (X_N, Y_N))$ be training examples. The model parameters $\mathbf{w}$ are learned using structured SVMs [40] by minimizing a quadratic objective function subject to a set of linear soft margin constraints,

$$\min_{\mathbf{w}, \boldsymbol{\xi}} \frac{1}{2} \|\mathbf{w}\|^2 + C \sum_{i=1}^{N} \xi_i \tag{11}$$
$$\text{s.t. } \forall i, Y \in \mathscr{Y}_{X_i} : \langle \mathbf{w}, \delta \Psi_i(Y) \rangle \geq \Delta(Y_i, Y) - \xi_i,$$

where $\delta \Psi_i(Y)$ denotes $\Psi(X_i, Y_i) - \Psi(X_i, Y)$ (thus $\langle \mathbf{w}, \delta \Psi_i(Y) \rangle = S(X_i, Y_i; \mathbf{w}) - S(X_i, Y; \mathbf{w})$) and the loss function $\Delta(Y_i, Y)$ in this case is simply the number of mislabeled nodes (photos) in the sequence. It is easy to see that the structured SVM degenerates into a multiclass SVM if every example has only a single node.

The difficulty of this formulation is that the label space $\mathscr{Y}_{X_i}$ grows exponentially with the length of the sequence X_i. Structured SVMs address this problem by iteratively minimizing the objective function using a cutting-plane algorithm, which requires finding the *most violated constraint* for every training exemplar at each iteration. Since the loss function $\Delta(Y_i, Y)$ decomposes into a sum over individual nodes, the most violated constraint,

$$\hat{Y}_i = arg\,max_{Y \in \mathscr{Y}_{X_i}} S(X_i, Y; \mathbf{w}) + \Delta(Y_i, Y), \tag{12}$$

can be obtained efficiently via Viterbi decoding.

4.3 Image Classification with Deep Learning

Since our original work on landmark recognition [23], a number of new approaches to object recognition and image classification have been proposed. Perhaps none has been as sudden or surprising as the very recent resurgence of interest in deep Convolutional Neural Networks, due to their performance on the 2012 ImageNet visual recognition challenge [9] by Krizhevsky *et al.* [20]. The main advantage of these techniques seems to be the ability to learn image features and image classifiers together in one unified framework, instead of creating the image features by hand (*e.g.* by using SIFT) or learning them separately.

To test these emerging models on our dataset, we trained networks using Caffe [17]. We bypassed the complex engineering involved in designing a deep network by starting with the architecture proposed by Krizhevsky *et al.* [20], composed of five convolutional layers followed by three fully connected layers. Mechanisms for contrast normalization and max pooling occur between many of the convolutional layers. Altogether the network contains around 60 million parameters; although our dataset is sufficiently large to train this model from random initialization, we choose instead to reduce training time by following Oquab *et al.* [29] and others by initializing from a pre-trained model. We modify the final fully connected layer to accommodate the appropriate number of categories for each task. The initial weights for these layers are randomly sampled from a zero-mean normal distribution.

Each model was trained using stochastic gradient descent with a batch size of 128 images. The models were allowed to continue until 25,000 batches had been processed with a learning rate starting at 0.001 which decayed by an order of magnitude every 2,500 batches. In practice, convergence was reached much sooner. Approximately 20% of the training set was withheld to avoid overfitting, and the training iteration with the lowest validation error was used for evaluation on the test set.

5 Experiments

We now present experimental results on our dataset of nearly 2 million labeled images. We created training and test subsets by dividing the *photographers* into two evenly-sized groups and then taking all photos by the first group as training images and all photos by the second group as test images. Partitioning according to user reduces the chance of 'leakage' between training and testing sets, for instance due to a given photographer taking nearly identical photos that end up in both sets.

We conducted a number of classification experiments with various subsets of the landmarks. The number of photos in the dataset differs widely from category to category; in fact, the distribution of photos across landmarks follows a power-law distribution, with the most popular landmark having roughly four times as many images as the 50th most popular landmark, which in turn has about four times as many images as the 500th most popular landmark. To ease comparison across different numbers of categories, for each classification experiment we subsample so that the number of images in each class is about the same. This means that the number of images in an m-way classification task is equal to m times the number of photos in the least popular landmark, and the probability of a correct random guess is $1/m$.

5.1 Bag of Words Models

Table 2 and Figure 2 present results for various classification experiments. For single image classification, we train three multiclass SVMs for the visual features, textual features, and the combination. For text features we use the normalized counts of text tags that are used by more than two photographers. When combining image and text features, we simply concatenate the two feature vectors for each photo. We see that classifying individual images using the bag-of-words visual models (as described

Table 2 Classification accuracy (% of images correct) for varying categories and types of models.

	Random	Images - BoW			Photo streams			Images - deep
Categories	**baseline**	visual	text	vis+text	visual	text	vis+text	visual
Top 10 landmarks	10.00	57.55	69.25	80.91	68.82	70.67	82.54	81.43
Landmark 200-209	10.00	51.39	79.47	86.53	60.83	79.49	87.60	72.18
Landmark 400-409	10.00	41.97	78.37	82.78	50.28	78.68	82.83	65.20
Human baseline	10.00	68.00	—	76.40	—	—	—	68.00
Top 20 landmarks	5.00	48.51	57.36	70.47	62.22	58.84	72.91	72.10
Landmark 200-219	5.00	40.48	71.13	78.34	52.59	72.10	79.59	63.74
Landmark 400-419	5.00	29.43	71.56	75.71	38.73	72.70	75.87	54.60
Top 50 landmarks	2.00	39.71	52.65	64.82	54.34	53.77	65.60	62.28
Landmark 200-249	2.00	27.45	65.62	72.63	37.22	67.26	74.09	55.87
Landmark 400-449	2.00	21.70	64.91	69.77	29.65	66.90	71.62	49.11
Top 100 landmarks	1.00	29.35	50.44	61.41	41.28	51.32	62.93	52.52
Top 200 landmarks	0.50	18.48	47.02	55.12	25.81	47.73	55.67	39.52
Top 500 landmarks	0.20	9.55	40.58	45.13	13.87	41.02	45.34	23.88

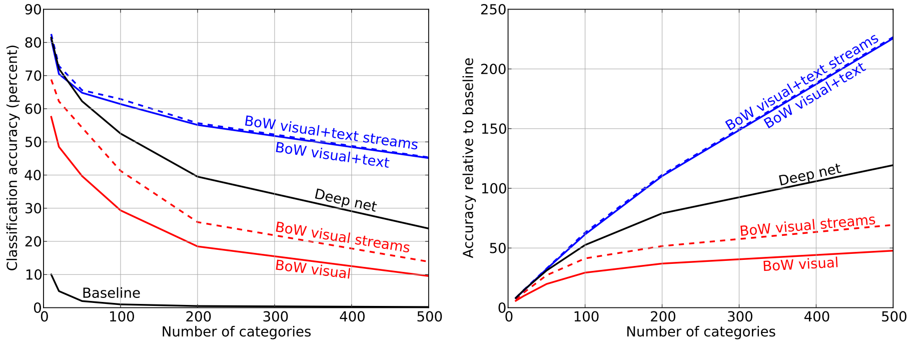

(a) (b)

Fig. 2 Classification accuracy for different types of models across varying numbers of categories, measured by (a) absolute classification accuracy; and (b) ratio relative to random baseline.

in Section 4.1) gives results that are less accurate than textual tags but nevertheless significantly better than random baseline — four to six times higher for the 10 category problems and nearly 50 times better for the 500-way classification. The combination of textual tags and visual tags performs significantly better than either alone, increasing performance by about 10 percentage points in most cases. This performance improvement is partially because about 15% of photos do not have any text tags. However, even when such photos are excluded from the evaluation, adding visual features still gives a significant improvement over using text tags alone, increasing accuracy from 79.2% to 85.47% in the top-10 category case, for example.

Table 2 shows classification experiments for different numbers of categories and also for categories of different rank. Of course, top-ranked landmark classes have (by definition) much more training data than lower-ranked classes, so we see sig-

Table 3 Visual classification rates for different vocabulary sizes.

	Vocabulary size				
# categories	**1,000**	**2,000**	**5,000**	**10,000**	**20,000**
10	47.51	50.78	52.81	55.32	57.55
20	39.88	41.65	45.02	46.22	48.51
50	29.19	32.58	36.01	38.24	39.71
100	19.77	24.05	27.53	29.35	30.42

nificant drops in visual classification accuracy when considering less-popular landmarks (e.g. from 57.55% for landmarks ranked 1–10 to 41.97% for those ranked 400–409). However for the text features, problems involving *lower-ranked* categories are actually *easier*. This is because the top landmarks are mostly located in the same major cities, so that tags like *london* are relatively uninformative. Lower categories show much more geo-spatial variation and thus are easier for text alone.

For most of the experiments shown in Figure 2, the visual vocabulary size was set to 20,000. This size was computationally prohibitive for our structured SVM learning code for the 200- and 500-class problems, so for those we used 10,000 and 5,000, respectively. We studied how the vocabulary size impacts classification performance by repeating a subset of the experiments for several different vocabulary sizes. As Table 3 shows, classification performance improves as the vocabulary grows, but the relative effect is more pronounced as the number of categories increases. For example, when the vocabulary size is increased from 1,000 to 20,000, the relative performance of the 10-way classifier improves by about 20% (10.05 percentage points, or about one baseline) while the accuracy of the 100-way classifier increases by more than 50% (10.65 percentage points, or nearly 11 baselines). Performance on the 10-way problem asymptotes by about 80,000 clusters at around 59.3%. Unfortunately, we could not try such large numbers of clusters for the other tasks, because the learning becomes intractable.

In the experiments presented so far we sampled from the test and training sets to produce equal numbers of photos for each category in order to make the results easier to interpret. However, our approach does not depend on this property; when we sample from the actual photo distribution our techniques still perform dramatically better than the majority class baseline. For example, in the top-10 problem using the actual photo distribution we achieve 53.58% accuracy with visual features and 79.40% when tags are also used, versus a baseline of 14.86%; the 20-way classifier produces 44.78% and 69.28% respectively, versus a baseline of 8.72%.

5.2 Human Baselines

A substantial number of Flickr photos are mislabeled or inherently ambiguous — a close-up photo of a dog or a sidewalk could have been taken at almost any landmark. To try to gauge the frequency of such difficult images, we conducted a small-scale, human-subject study. We asked 20 well-traveled people each to label 50 photos taken in our top-10 landmark dataset. Textual tags were also shown for a random subset of the photos. We found that the average human classification accuracy was 68.0% without textual tags and 76.4% when both the image and tags were shown (with standard deviations of 11.61 and 11.91, respectively). Thus the humans performed better than the automatic classifier when using visual features alone (68.0% versus 57.55%) but about the same when both text and visual features were available (76.4% versus 80.91%). However, we note that this was a small-scale study and not entirely fair: the automatic algorithm was able to review hundreds of thousands of training images before making its decisions, whereas the humans obviously could not. Nevertheless, the fact that the human baseline is not near 100% gives some indication of the difficulty of this task.

5.3 Classifying Photo Streams

Table 2 and Figure 2 also present results when temporal features are used jointly to classify photos nearby in time from the same photographer, using structured SVMs, as described in Section 4.2. For training, we include only photos in a user's photostream that are within one of the categories we are considering. For testing, however, we do not assume such knowledge (because we do not know where the photos were taken ahead of time). Hence the photo streams for testing may include photos outside the test set that do not belong to any of the categories, but only photos in the test set contribute towards evaluation. For these experiments, the maximum length of a photo stream was limited to 11, or five photos before and after a photo of interest.

The results show a significant improvement in visual bag-of-words classification when photo streams are classified jointly — nearly 12 percentage points for the top-10 category problem, for example. In contrast, the temporal information provides little improvement for the textual tags, suggesting that tags from contemporaneous images contain largely redundant information. In fact, the classification performance using temporal and visual features is actually slightly higher than using temporal and textual features for the top-20 and top-50 classification problems. For all of the experiments, the best performance for the bag-of-words models is achieved using the full combination of visual, textual and temporal features, which, for example, gives 82.54% correct classification for the 10-way problem and 45.34% for the 500-way problem — more than 220 times better than the baseline.

5.4 Classifying with Deep Networks

Finally, we tested our problem on what has very recently emerged as the state-of-the-art in classification technology: deep learning using Convolutional Neural Networks. Figure 2 shows the results for the single image classification problem, using vision features alone. The CNNs perform startlingly well on this problem compared to the more traditional bag-of-words models. On the 10-way problem, they increase results by almost *25 percentage points*, or about 2.5 times the baseline, from 57.6% to 81.4%. In fact, CNNs with visual features significantly outperform the text features, and very narrowly beat the combined visual and text features. They also beat the photo stream classifiers for both text and visual features, despite the fact the CNNs see less information (a single image versus a stream of photos), and very slightly underperform when vision and text are both used. The CNNs also beat the humans by a large margin (81.4% versus 68.0%), even when the humans saw text tags and the CNNs did not (81.4% versus 76.4%).

For classification problems with more categories, CNNs outperform bag-of-words visual models by an increasing margin relative to baseline. For instance, for 50-way the CNN increases performance from 39.71% to 62.28%, or by more than 11 baselines, whereas for 500-way the increase is 9.55% to 23.88%, or over 71 baselines. However, as the number of categories grows, text features start to catch up with visual classification with CNNs, roughly matching it for the 100-way problem and significantly beating for 500-way (40.58% vs 23.88%). For 500-way, the combined text and vision using bags-of-words outperform the vision-only CNNs by a factor of about 2 (45.13% vs 23.88%). Overall, however, our results add to evidence that deep learning can offer significant improvements over more traditional techniques, especially on image classification problems where training sets are large.

5.5 Discussion

The experimental results we report here are highly precise because of the large size of our test dataset. Even the smallest of the experiments, the top-10 classification, involves about 35,000 test images. To give a sense of the variation across runs due to differences in sampling, we ran 10 trials of the top-10 classification task with different samples of photos and found the standard deviation to be about 0.15 percentage points. Due to computational constraints we did not run multiple trials for the experiments with large numbers of categories, but the variation is likely even less due to the larger numbers of images involved.

We showed that for the top-10 classification task, our automatic classifiers can produce accuracies that are competitive with or even better than humans, but are still far short of the 100% performance that we might aspire to. To give a sense for the error modes of our classifiers, we show a confusion matrix for the CNNs on the 10-way task in Figure 3. The four most difficult classes are all in London (Trafalgar Square, Big Ben, London Eye, Tate Modern), with a substantial degree of confusion between them (especially between Big Ben and London Eye). Classes within the same city can be confusing because it is often possible to either photograph two landmarks in the same photo, or to photograph one landmark from the other. Landmarks in the same city also show greater noise in the ground truth, since con-

	Predicted class									
Correct class	Eiffel	Trafalgar	Big Ben	London Eye	Notre Dame	Tate Modern	Empire State Bldg	Piazza San Marco	Colosseum	Louvre
Eiffel	**82.3**	2.2	1.0	2.7	2.4	2.3	3.0	1.1	0.7	1.7
Trafalgar	0.7	**77.0**	2.9	2.3	1.5	4.0	2.3	4.1	1.8	3.6
Big Ben	1.2	3.7	**76.8**	8.2	2.2	3.4	1.1	1.4	0.7	1.3
London Eye	2.9	2.9	8.1	**76.3**	1.4	2.6	2.2	1.3	0.5	1.7
Notre Dame	2.0	2.9	1.7	1.6	**81.8**	1.1	1.0	2.7	2.1	3.0
Tate Modern	1.6	3.2	1.7	3.4	1.3	**81.0**	2.4	1.7	1.2	2.6
Empire State Bldg	1.6	1.9	1.2	1.5	0.6	2.3	**88.2**	0.8	0.6	1.2
Piazza San Marco	1.3	4.1	0.9	1.1	2.8	2.0	1.7	**81.1**	2.1	2.9
Colosseum	0.9	1.7	0.6	0.5	2.0	1.4	0.4	2.1	**88.7**	1.6
Louvre	1.2	2.8	0.9	1.2	2.8	4.1	1.0	3.1	1.9	**81.5**

Fig. 3 Confusion matrix for the Convolutional Neural Network visual classifier, in percentages. Off-diagonal cells greater than 3% are highlighted in yellow, and greater than 6% are shown in red.

Correct:	Trafalgar Square	London Eye	Trafalgar Square	Notre Dame	Trafalgar Square
Predicted:	Colosseum	Eiffel Tower	Piazza San Marco	Eiffel Tower	Empire State Building
	(a)	(b)	(c)	(d)	(e)

Correct:	Tate Modern	Big Ben	Notre Dame	Louvre	Piazza San Marco
Predicted:	Louvre	Piazza San Marco	Big Ben	Notre Dame	London Eye
	(f)	(g)	(h)	(i)	(j)

Fig. 4 Random images incorrectly classified by the Convolutional Neural Network using visual features, on the 10-way problem.

sumer GPS is only accurate to a few meters under ideal circumstances, and signal reflections in cities can make the error significantly worse.

Figure 4 shows a random set of photos incorrectly classified by the CNN. Several images, like (c) and (i), are close-ups of objects that have nothing to do with the landmark itself, and thus are probably nearly impossible to identify even with an optimal classifier. Other errors seem quite understandable at first glance, but could probably be fixed with better classifiers and finer-grained analysis. For instance, image 4(a) is a close-up of a sign and thus very difficult to geo-localize, but a human would not have predicted Colosseum because the sign is in English. Image (e) is a crowded street scene and the classifier's prediction of Empire State Building is not unreasonable, but the presence of a double-decker bus reveals that it must be in London. Image (f) is a photo of artwork and so the classifier's prediction of the Louvre museum is understandable, although a tenacious human could have identified the artwork and looked up where it is on exhibit. This small study of error modes suggests that while some images are probably impossible to geo-localize correctly, our automatic classifiers are also making errors that, at least in theory, could be fixed by better techniques with finer-grained analysis.

Regarding running times, the bag-of-words image classification on a single 2.66 GHz processor took about 2.4 seconds, most of which was consumed by SIFT interest point detection. Once the SIFT features were extracted, classification required only approximately 3.06 ms for 200 categories and 0.15 ms for 20 categories. SVM training times varied by the number of categories and the number of features, ranging from less than a minute on the 10-way problems to about 72 hours for the 500-way structured SVM on a single CPU. We conducted our bag-of-words experiments on a small cluster of 60 nodes running the Hadoop open source map-reduce framework. The CNN image classification took approximately 4 milliseconds per image running on a machine equipped with an NVidia Tesla K20 GPU. Starting from the pretrained ImageNet model provided a substantial speedup for training the network, with convergence ranging between about 2 hours for 10 categories to 3.5 hours for the 500-way problem.

6 Summary

We have shown how to create large labeled image datasets from geotagged image collections, and experimented with a set of over 30 million images of which nearly 2 million are labeled. Our experiments demonstrate that multiclass SVM classifiers using SIFT-based bag-of-word features achieve quite good classification rates for large-scale problems, with accuracy that in some cases is comparable to that of humans on the same task. We also show that using a structured SVM to classify the stream of photos taken by a photographer, rather than classifying individual photos, yields dramatic improvement in the classification rate. Such temporal context is just one kind of potential contextual information provided by photo-sharing sites. When these image-based classification results are combined with text features from tagging, the accuracy can be hundreds of times the random guessing baseline. Finally, recent advances in deep learning have pushed the state of the art significantly, demonstrating dramatic improvements over the bags-of-words classification techniques. Together these results demonstrate the power of large labeled datasets and the potential for classification of Internet-scale image collections.

Acknowledgements The authors thank Alex Seewald and Dennis Chen for configuring and testing software for the deep learning experiments during a Research Experiences for Undergraduates program funded by the National Science Foundation (through CAREER grant IIS-1253549). The research was supported in part by the NSF through grants BCS-0537606, IIS-0705774, IIS-

0713185, and IIS-1253549, by the Intelligence Advanced Research Projects Activity (IARPA) via Air Force Research Laboratory, contract FA8650-12-C-7212, and by an equipment donation from NVidia Corporation. This research used the high-performance computing resources of Indiana University which are supported in part by NSF (grants ACI-0910812 and CNS-0521433), and by the Lilly Endowment, Inc., through its support for the Indiana University Pervasive Technology Institute, and in part by the Indiana METACyt Initiative. It also used the resources of the Cornell University Center for Advanced Computing, which receives funding from Cornell, New York State, NSF, and other agencies, foundations, and corporations. The U.S. Government is authorized to reproduce and distribute reprints for Governmental purposes notwithstanding any copyright annotation thereon. Disclaimer: The views and conclusions contained herein are those of the authors and should not be interpreted as necessarily representing the official policies or endorsements, either expressed or implied, of IARPA, AFRL, NSF, or the U.S. Government.

References

1. Arya, S., Mount, D.M.: Approximate nearest neighbor queries in fixed dimensions. In: ACM-SIAM Symposium on Discrete Algorithms (1993)
2. Bort, J.: Facebook stores 240 billion photos and adds 350 million more a day. In: Business Insider (2013)
3. Collins, B., Deng, J., Li, K., Fei-Fei, L.: Towards scalable dataset construction: An active learning approach. In: European Conference on Computer Vision (2008)
4. Comaniciu, D., Meer, P.: Mean shift: A robust approach toward feature space analysis. IEEE Transactions on Pattern Analysis and Machine Intelligence (2002)
5. Crammer, K., Singer, Y.: On the algorithmic implementation of multiclass kernel-based vector machines. Journal of Machine Learning Research (2001)
6. Crandall, D., Backstrom, L., Huttenlocher, D., Kleinberg, J.: Mapping the world's photos. In: International World Wide Web Conference (2009)
7. Crandall, D., Owens, A., Snavely, N., Huttenlocher, D.: SfM with MRFs: Discrete-continuous optimization for large-scale structure from motion. IEEE Transactions on Pattern Analysis and Machine Intelligence **35**(12) (2013)
8. Csurka, G., Dance, C., Fan, L., Willamowski, J., Bray, C.: Visual Categorization with Bags of Keypoints. In: ECCV Workshop on Statistical Learning in Computer Vision (2004)
9. Deng, J., Dong, W., Socher, R., Li, L., Li, K., Fei-Fei, L.: ImageNet: A large-scale hierarchical image database. In: IEEE Conference on Computer Vision and Pattern Recognition (2009)
10. Everingham, M., Van Gool, L., Williams, C.K.I., Winn, J., Zisserman, A.: The PASCAL VOC 2008. http://www.pascal-network.org/challenges/VOC/voc2008/workshop/
11. Girshick, R., Donahue, J., Darrell, T., Malik, J.: Rich feature hierarchies for accurate object detection and semantic segmentation. arXiv preprint arXiv:1311.2524 (2013)
12. Grauman, K., Leibe, B.: Visual Object Recognition. Morgan & Claypool Publishers (2011)
13. Griffin, G., Holub, A., Perona, P.: Caltech-256 object category dataset. Tech. rep., California Institute of Technology (2007)
14. Hao, Q., Cai, R., Li, Z., Zhang, L., Pang, Y., Wu, F.: 3d visual phrases for landmark recognition. In: IEEE Conference on Computer Vision and Pattern Recognition (2012)
15. Hauff, C.: A study on the accuracy of Flickr's geotag data. In: International ACM SIGIR Conference (2013)
16. Hays, J., Efros, A.A.: IM2GPS: Estimating geographic information from a single image. In: IEEE Conference on Computer Vision and Pattern Recognition (2008)
17. Jia, Y.: Caffe: An open source convolutional architecture for fast feature embedding. http://caffe.berkeleyvision.org/ (2013)
18. Joachims, T.: Making large-scale SVM learning practical. In: B. Schölkopf, C. Burges, A. Smola (eds.) Advances in Kernel Methods - Support Vector Learning. MIT Press (1999)

19. Kalogerakis, E., Vesselova, O., Hays, J., Efros, A., Hertzmann, A.: Image sequence geolocation with human travel priors. In: IEEE International Conference on Computer Vision (2009)
20. Krizhevsky, A., Sutskever, I., Hinton, G.: ImageNet classification with deep convolutional neural networks. In: Advances in Neural Information Processing Systems (2012)
21. Lee, S., Zhang, H., Crandall, D.: Predicting geo-informative attributes in large-scale image collections using convolutional neural networks. In: IEEE Winter Conference on Applications of Computer Vision (2015)
22. Li, X., Wu, C., Zach, C., Lazebnik, S., Frahm, J.: Modeling and recognition of landmark image collections using iconic scene graphs. In: European Conference on Computer Vision (2008)
23. Li, Y., Crandall, D., Huttenlocher, D.: Landmark classification in large-scale image collections. In: IEEE International Conference on Computer Vision (2009)
24. Li, Y., Snavely, N., Huttenlocher, D., Fua, P.: Worldwide pose estimation using 3d point clouds. In: European Conference on Computer Vision (2012)
25. Lowe, D.G.: Distinctive image features from scale-invariant keypoints. International Journal of Computer Vision **60**(2), 91–110 (2004)
26. Luo, J., Joshi, D., Yu, J., Gallagher, A.: Geotagging in multimedia and computer vision – a survey. Multimedia Tools and Applications **51**(1), 187–211 (2011)
27. McAuley, J.J., Leskovec, J.: Image labeling on a network: Using social-network metadata for image classification. In: ECCV (2012)
28. Miller, G.: WordNet: A lexical database for English. Communications of the ACM **38**(11), 39–41 (1995)
29. Oquab, M., Bottou, L., Laptev, I., Sivic, J.: Learning and transferring mid-level image representations using convolutional neural networks. In: CVPR (2014)
30. Philbin, J., Chum, O., Isard, M., Sivic, J., Zisserman, A.: Object retrieval with large vocabularies and fast spatial matching. In: IEEE Conference on Computer Vision and Pattern Recognition (2007)
31. Raguram, R., Tighe, J., Frahm, J.M.: Improved geometric verification for large scale landmark image collections. In: British Machine Vision Conference (2012)
32. Razavian, A.S., Azizpour, H., Sullivan, J., Carlsson, S.: CNN features off-the-shelf: an astounding baseline for recognition. arXiv preprint arXiv:1403.6382 (2014)
33. Schroff, F., Criminisi, A., Zisserman, A.: Harvesting image databases from the web. In: IEEE International Conference on Computer Vision (2007)
34. Sermanet, P., Eigen, D., Zhang, X., Mathieu, M., Fergus, R., LeCun, Y.: Overfeat: Integrated recognition, localization and detection using convolutional networks. CoRR **abs/1312.6229** (2013). URL http://arxiv.org/abs/1312.6229
35. Snavely, N., Seitz, S.M., Szeliski, R.: Modeling the World from Internet Photo Collections. International Journal of Computer Vision **80**(2) (2008)
36. Stone, Z., Zickler, T., Darrell, T.: Autotagging Facebook: Social network context improves photo annotation. In: 1st IEEE Workshop on Internet Vision (2008)
37. Taigman, Y., Yang, M., Ranzato, M., Wolf, L.: DeepFace: Closing the gap to human-level performance in face verification. In: IEEE Conference on Computer Vision and Pattern Recognition (2013)
38. Torralba, A., Efros, A.: Unbiased look at dataset bias. In: IEEE Conference on Computer Vision and Pattern Recognition (2011)
39. Toshev, A., Szegedy, C.: DeepPose: Human pose estimation via deep neural networks. arXiv preprint arXiv:1312.4659 (2013)
40. Tsochantaridis, I., Hofmann, T., Joachims, T., Altun, Y.: Support vector machine learning for interdependent and structured output spaces. In: International Conference on Machine Learning (2004)
41. Zeiler, M.D., Fergus, R.: Visualizing and understanding convolutional networks. In: European Conference on Computer Vision (2014)
42. Zheng, Y., Zhao, M., Song, Y., Adam, H., Buddemeier, U., Bissacco, A., Brucher, F., Chua, T., Neven, H.: Tour the world: building a web-scale landmark recognition engine. In: IEEE Conference on Computer Vision and Pattern Recognition (2009)